Distribution Category:
Magnetic Fusion Energy
(UC-20)

ANL/FPP/TM-192

ANL/FPP/TM--192

DE85 009790

ARGONNE NATIONAL LABORATORY
9700 South Cass Avenue
Argonne, Illinois 60439

MODELING OF LIQUID-METAL CORROSION/DEPOSITION IN A FUSION REACTOR BLANKET

by

S. Malang* and D. L. Smith

Fusion Power Program

April 1984

* Visiting Scientist, 1983. Present address: Kernforschungszentrum Karlsruhe, Postfach 3640, 7500 Karlsruhe, Federal Republic of Germany.

TABLE OF CONTENTS

TABLE OF CONTENTS (Contd.)

LIST OF FIGURES

LIST OF TABLES

MODELING OF LIQUID-METAL CORROSION/DEPOSITION IN A FUSION REACTOR BLANKET

by

S. Malang and D. L. Smith

ABSTRACT

A model has been developed for the investigation of the liquid-metal corrosion and the corrosion product transport in a liquid-metal-cooled fusion reactor blanket. The model describes the two-dimensional transport of wall material in the liquid-metal flow and is based on the following assumptions:

- Parallel flow in a straight circular tube.
- Transport of wall material perpendicular to the flow direction by diffusion and turbulent exchange; in flow direction by the flow motion only.
- Magnetic field causes uniform velocity profile with thin boundary layer and suppresses turbulent mass exchange.
- Liquid metal at the interface is saturated with wall material.

A computer code based on this model has been used to analyze the corrosion of ferritic steel by lithium lead and the deposition of wall material in the cooler part of a loop.

Three cases have been investigated: (1) ANL forced convection corrosion experiment (without magnetic field), (2) corrosion in the MARS liquid-metal-cooled blanket (with magnetic field), and (3) deposition of wall material in the corrosion product cleanup system of the MARS blanket loop.

The evaluations showed that the code can be used to analyze, at least qualitatively, the influence of the most important parameters, including a magnetic field, on the corrosion and deposition rate.

1. INTRODUCTION

Liquid lithium and an eutectic lithium-lead alloy are attractive breeder materials in fusion reactors operating on a D-T fuel cycle. These metals are known, however, as much more corrosive than the sodium in a liquid metal fast breeder reactor (LMFBR) if austenitic or ferritic steels are used as the structure material.

In some concepts the liquid metal is used as breeder only, cooled by water or helium and circulated slowly for tritium recovery. In other concepts, the liquid metal is used as both breeder and as coolant. Especially in the self-cooled case the velocity of the liquid metal is a very important design parameter since it has a large influence on:

- MHD - pressure drop
- cooling of the first wall
- corrosion rate.

The MHD pressure drop, in particular, limits the allowable velocity perpendicular to the magnetic field to values below 0.5 m/s. This results in relatively large flow areas and in rather short flow path length.

The main differences in the liquid metal corrosion in a fusion reactor blanket compared to a LMFBR can be summarized as follows:

- liquid metal more corrosive
- influence of magnetic field on flow profiles
- lower velocity
- smaller length/diameter ratio of channel.

The effects of the magnetic field in particular makes it difficult to predict the corrosion and deposition behavior in a fusion reactor blanket by using the experience and the models developed for LMFBRs. It is not known in the case of a fusion reactor blanket whether the magnetic field increases or decreases the corrosion rate.

The corrosion rate of austenitic and ferritic steels in lithium environment has been measured in a number of experiments.[1,2,3] These experiments, however, do not provide a quantitative correlation of the corrosion rate to the flow rate and the temperature gradient in the loop.

The data are more limited in lithium-lead environment[4] and no experiments have been conducted to determine the influence of a magnetic field on the corrosion rate.

Measured deposition rates in either lithium or lithium-lead are even more scarce than corrosion rates. Liquid-metal loops are generally not designed to investigate deposition characteristics. These effects are generally evaluated only if there is a problem such as plugging. In most cases, it is not possible to correlate the deposition to the loop parameters since the parameters are frequently changed. Sometimes the loops are constructed of more than one material and frequently different materials are added as corrosion specimens. This makes it nearly impossible to correlate the corrosion or deposition rate to the kind and amount of wall materials in solution.

It is generally agreed that there are more variables influencing the corrosion and deposition rates than can be investigated experimentally. Also, there is a need for modeling work; however, one must be careful not to overestimate the value of a model since it is not possible to predict absolute values without correlations with benchmark experiments.

The purpose of this study was to develop a model which can be used to analyze the influence of the parameters that affect the corrosion and deposition behavior in a liquid-metal blanket.

2. PROBLEM DEFINITION

Corrosion of materials by liquid metals is a very complex process in which a number of different phenomena contribute to the overall corrosion rate. The most important principal processes involved are:[5]

- dissolution
- alloying
- intergranular penetration
- impurity transfer from or to the liquid metal
- leaching out of wall material components
- transport of wall material in the liquid metal by molecular diffusion.

In some systems the corrosion rate is controlled predominantly by a single phenomena, but, in general, a combination of processes must be considered.

The scope of this study is limited to the transport phenomena inside the liquid metal. No attempt has been made to model changes in the wall composition near the surface or to consider more than one component diffusing in the liquid metal. This clearly limits the direct applicability of the model either to ferritic wall materials or, in the case of austenitic steels, to the steady state region after an initial period of high dissolution rate. Heat transport could be analyzed by using the same models as developed for the mass transport but the temperature calculation has been omitted from simplicity.

The main objective of the study was to investigate the influence of the following parameters on the corrosion and deposition rates:

- mass flux
- velocity profile
- turbulence
- magnetic field
- tube length and tube diameter
- heat up rate
- concentration of the wall material in the liquid metal.

It is recognized that the results can show only the relative importance of the particular parameter. To predict absolute values, the model must be verified with suitable experiments. Nevertheless, the model should provide upper limits for the corrosion and deposition rates if applied to a particular blanket and liquid metal loop design.

3. CORROSION PRODUCT TRANSPORT MODEL

The modeling work has focused on the development of a computer code that describes the two-dimensional transport of corrosion products in liquid metal flow. A straight tube with circular cross section is used as basic geometry. Fully developed steady state flow is assumed with the velocity profile and the turbulence dependent on the Reynolds number and on the presence or absence of a magnetic field.

The concentration of wall material is calculated as functions of the radius and the coordinate in the axial direction. The concentration profile is then used to determine the corrosion rate and the mass transfer coefficient for comparison with less detailed models.

3.1 Assumptions

The basic assumption of the model is that the transport of the wall material in the liquid metal is the rate determining step. For systems where this is not the case, the use of the model is rather limited. In contrast to this inherent assumption the following ones could be lifted in later versions:

(a) The wall is corroded uniformly and the wall material is treated as one component only.

(b) The liquid metal at the wall surface is always saturated with wall material.

3.1.1 Uniform Corrosion

This is generally not the case in the initial period if austenitic steels are used as structural materials. The high solubility of nickel in lithium as well as in lithium-lead results in a decrease of the nickel concentration in the wall near the surface and leads finally to the formation of a ferritic layer. As long as this layer is closed and the material transport in this layer is by diffusion, a non-steady state model could be added to calculate the concentration profile in the wall.[6]

If the layer is porous and weak as it is the case for the combination austenitic steel/lithium-lead,[4] the corrosion rate is so high that this combination is not interesting at all.

There is experimental evidence, however, that the assumption of uniform corrosion is justified for ferritic steels in lithium as well as in lithium-lead and in addition for austenitic steels in lithium during the steady state phase.

3.1.2 Liquid Metal Is Saturated at Interface

The assumption that the liquid metal is saturated at the interface is the most important shortcoming of the present model as well as many other previous

models. This assumption leads in all cases to an overestimation of the corrosion rate. Although poor agreement of model predictions with experimental observations is frequently attributed to errors associated with this assumption, in many cases the disagreement between prediction and experiment can be attributed predominantly to other assumptions, e.g. variations in flow profile. This shall be explained using the basic mass transfer equation, written for one component only.

$$\dot{m} = K_m \cdot (C_I - \bar{C}) , \qquad (1)$$

where

$\dot{m}$ = mass transfer rate

K_m = mass transfer coefficient

C_I = concentration of the transferred component at the interface

$\bar{C}$ = average concentration in the fluid cross section.

All three independent variables in Eq. (1) can contribute to a deviation between predicted and measured corrosion rates.

The transfer coefficient K_m depends on the flow conditions and the properties of the liquid metal but is for given flow conditions considerably higher in the entrance region than for a fully developed concentration profile. In fluids with high Schmidt numbers, i.e. liquid metals, the development of the concentration profile takes a flow path length much longer than the development of the velocity profile or the temperature profile.[7] This is especially true in laminar flow and in cases where the wall concentration changes in flow directions. Many mass transfer models neglect the entrance region, leading to an underestimation of the corrosion rate.

The bulk concentration $\bar{C}$ is assumed as zero in a number of models because the solubility of wall materials in the liquid metal is small. But in real cases this concentration can build up with time and it may approach the saturation concentration at the highest loop temperature.

These facts must be considered if Eq. (1) is used for the prediction of the mass transfer rate. There is no doubt, however, that the interface concentration C_I can be lower (in the case of corrosion) or higher (in the case

of deposition) than the saturation concentration. This is caused by a resistance at the interface if a material is dissoluted or segregated as described by Eq. (2).

$$\dot{m} = K_D \cdot (C_s - C_I) , \tag{2}$$

where

K_D = dissolution (or segregation) coefficient

C_s = saturation concentration

Dissolution and segregation processes are very complex and difficult to describe quantitatively. In general, K_D, which must be determined experimentally depends on the mass transfer rate itself. This is not the case with the mass transfer coefficient K_m. Usually the assumption is made that $K_D \gg K_m$ and therefore $C_I \equiv C_s$. This leads to an overestimation of the mass transfer rate and has to be justified on a case to case basis.

In the study presented here the assumption of saturation at the interface has an influence on the agreement between measured and calculated corrosion rates, but it has no impact on the relative importance of the parameters investigated here.

3.2 Determination of Velocity and Concentration Profiles

The transport of wall material in the liquid metal perpendicular to the wall is by diffusion, whereas transport parallel to the wall is by convection. Diffusion can be molecular or turbulent. Diffusion and transport by convection are strongly influenced by the flow pattern (laminar or turbulent) and by a magnetic field. Therefore, the velocity profile and the turbulent eddy mass diffusivity have to be determined prior to the calculation of the concentration profile.

3.2.1 Velocity Profile

The flow pattern is determined by the Reynolds number.

$$Re = \frac{\bar{v} \cdot d}{\nu} , \tag{3}$$

where

$\bar{v}$ = mean velocity

d = tube diameter

ν = kinematic viscosity

3.2.1.1 Laminar Flow

If the actual Reynolds number is smaller than a critical value, the flow is laminar with a parabolic velocity profile. The critical Reynolds number for flow in tubes is 2320.

$$\frac{v(r)}{\bar{v}} = 2 \cdot [1 - (r/R)^2] , \tag{4}$$

where R = tube radius.

3.2.1.2 Turbulent Flow

There is a transition region between the laminar and the turbulent region. For simplicity, this transition region is neglected here and the flow is treated as either laminar or turbulent. In the turbulent case the tube cross section is divided into a laminar sublayer, a buffer zone and a turbulent core. A dimensionless wall distance is calculated and used to determine the thickness of the different regions:

$$y^+ = (y/\nu) \sqrt{\tau_o/\rho_o} , \tag{5}$$

where

y = distance from the wall

ν = kinematic viscosity

τ_o = shear stress at the wall

ρ = fluid density.

The term $\sqrt{\tau_o/\rho}$ is called the friction velocity and can be rewritten to

$$v^* = \sqrt{\tau_o/\rho} = \bar{v} \cdot \sqrt{f/8} . \tag{6}$$

The friction factor f is calculated with the Blasius formula for smooth pipes.

$$f = 0.3164\ Re^{-0.25} . \tag{7}$$

The dividing lines between the flow regions are set as follows:

$0 \leq y^+ \leq 5$	laminar sublayer
$5 < y^+ \leq 30$	buffer zone
$30 < y^+$	turbulent core

A so-called universial velocity distribution is used in determining velocity profile. This velocity profile can be written in terms of a dimensionless velocity v^+:

$$0 \leq y^+ \leq 5 \qquad v^+ = y^+ \tag{8a}$$

$$5 < y^+ \leq 30 \qquad v^+ = 5.0 \cdot \ln y^+ - 3.05 \tag{8b}$$

$$30 < y^+ \qquad v^+ = 2.5 \cdot \ln y^+ + 5.5 \tag{8c}$$

The actual velocity is then

$$v = v^+ \cdot v^* , \tag{9}$$

with the friction velocity as defined in Eq. (6).

3.2.1.3 Flow in a Magnetic Field

The magnetic field causes the velocity profile to become very flat. For the purpose of this study slug flow has been assumed where the velocity is constant across the tube with the exception of a thin boundary layer. The velocity increases linearly in the boundary layer. A second result of the magnetic field is the suppression of all turbulent exchange.

3.2.2 Molecular and Turbulent Diffusivity

In general the diffusivity is the sum of a molecular and a turbulent part:

$$D = D_{molecular} + D_{turbulent} . \tag{10}$$

As a first approach the molecular diffusivity $D_{molecular}$ *can be predicted by* the Stoke's-Einstein equation:

$$D_{molecular} = \frac{K \cdot T}{G \cdot \pi \cdot \mu \cdot R_i} , \tag{11}$$

where

K = Bolzmann's constant

T = absolute temperature

μ = dynamic viscosity

R_i = particle radius (here radius of the wall atom).

Another name for the turbulent diffusivity $D_{turbulent}$ is eddy mass diffusivity. There are a number of theories and equations to predict the value of this variable.[6,7]

The turbulent mass transfer plays an important part if water or gases are used as fluids. In fluids with a high Schmidt number, however, e.g. liquid metals, the mass transfer is governed mainly by the molecular diffusion in the laminar sublayer. Therefore, no effort has been made to select the most precise equations for determining the turbulent diffusivity. A constant value is used in the turbulant core, depending on the Reynolds number.

$$30 < y^+ : D_{turbulent} = 0.005 \cdot \nu \cdot Re^{0.875} . \tag{12}$$

For the buffer zone the turbulent diffusivity is calculated to

$$5 < y^+ \leq 30 : D_{turbulent} = \nu(y^+/5 - 1) . \tag{13}$$

3.2.3 Concentration Profile

The concentration field in a non-moving system can be described by the following equation:[8]

$$VN = \frac{\partial C}{\partial t} . \tag{14}$$

In an axially symmetrical case, i.e. a circular straight tube, Eq. (14) can be written in the form

$$\frac{\partial N_r}{\partial r} + \frac{N_r}{r} + \frac{\partial N_z}{\partial z} = -\frac{\partial C}{\partial t} \tag{15}$$

where C is the concentration of the diffusing material, N_r and N_z the mass fluxes of this material. The mass fluxes from diffusion are described by Fick's first law.[9]

$$N_r = -D_r \cdot \frac{\partial C}{\partial r} \tag{16a}$$

$$N_z = -D_z \cdot \frac{\partial C}{\partial z} . \tag{16b}$$

If there is mass transport by convection in addition to the mass transport by diffusion, an convective term has to be added to Eq. (16):

$$N_r = -D_r \cdot \frac{\partial C}{\partial r} + C \cdot v_r \tag{17a}$$

$$N_z = -D_z \cdot \frac{\partial C}{\partial Z} + C \cdot v_z . \tag{17b}$$

Some simplifications of Eqs. (15) and (17) can be made for the problem investigated here.

(a) $\frac{\partial C}{\partial t} = 0$ steady state

(b) $v_r = 0$ one-dimensional flow

(c) $D_z \cdot \frac{\partial C}{\partial z} = 0$ diffusion in axial direction neglected.

The remaining system of equation is

$$\frac{\partial N_r}{\partial r} + \frac{N_r}{r} + \frac{\partial N_z}{\partial z} = 0 \tag{18}$$

$$N_r = -D \cdot \frac{\partial C}{\partial r} \tag{19}$$

$$N_z = C \cdot v \cdot \tag{20}$$

The velocity v is determined by Eqs. (4) and (8) for laminar flow and turbulent flow, respectively. These equations must be solved in order to obtain the concentration profiles as functions of the axial coordiate z. Analytical solutions are available for very restricted cases. These restrictions are:

(a) laminar flow only;

(b) boundary condition at the outer surface either constant concentration (independent of z) or constant mass flux over the entire length; and

(c) constant diffusivity D in the entire region.

These restrictions make analytical solutions inapplicable to the problem investigated here. Therefore, a finite difference method has been chosen.[10] To use this method a network of grid points has to be established throughout the flow region. Difference equations have to be written, describing the concentration in the grid points. In setting up the difference equations, an engineer's approach is used by writing mass balances rather than to deal mathematically with partial differential equations. This shall be explained with the help of Fig. 1.

The mass balance for the grid point i,j having the concentration $C_{i,j}$ is:

$$N_r(i-1,j) - N_r(i,j) + N_z(i,j-1) - N_z(i,j) = 0 \tag{21}$$

$$N_r(i-1,j) = D_{i-1,j} \frac{0.5(\Delta z_{j-1} + \Delta z_j)(r_{i-1} + r_i)\pi(C_{i-1,j} - C_{i,j})}{\Delta r_{i-1}} \tag{22a}$$

$$N_z(i,j) = D_{i,j} \frac{0.5(\Delta z_{j-1} + \Delta z_j)(r_i + r_{i+1})\pi(C_{i,j} - C_{i+1,j})}{\Delta r_i} \tag{22b}$$

$$N_z(i,j-1) = v_i \cdot 0.5(\Delta r_{i-1} + \Delta r_i) \cdot 2 \cdot r_i \cdot \pi \cdot C_{i,j-1} \tag{23a}$$

$$N_z(i,j) = v_i \cdot 0.5(\Delta r_{i-1} + \Delta r_i) \cdot 2 \cdot r_i \cdot \pi \cdot C_{i,j} \tag{23b}$$

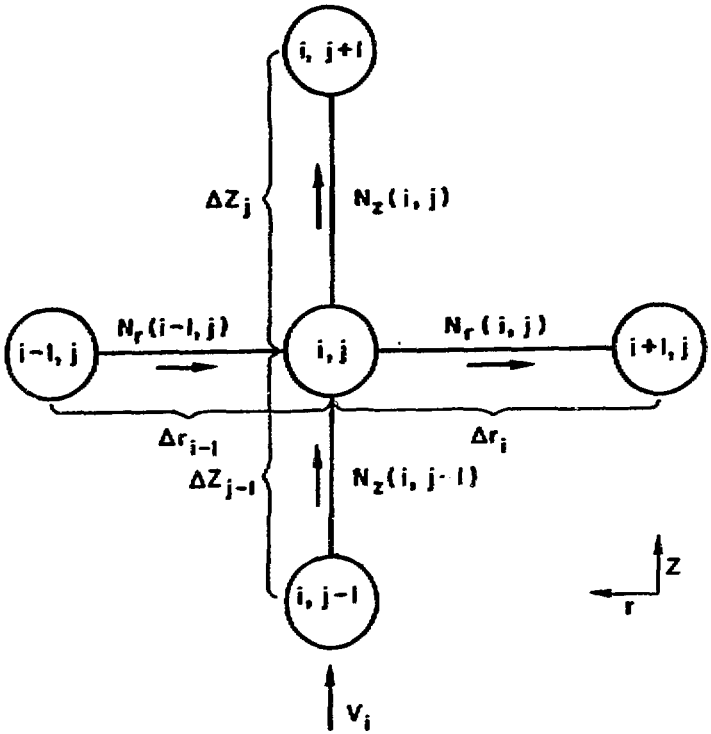

Fig. 1. Discrete approximation of the continuous two-dimensional region.

The mass balances for all grid points together lead to a matrix which has to be solved for the unknown concentrations $C_{i,j}$, using appropriate boundary conditions.

3.2.4 Boundary Conditions

It is assumed that the concentration C is uniform across the tube inlet.

$$C\,(r,0) = C_0 \qquad \begin{cases} z = 0 \\ 0 \leq r \leq R \end{cases} . \tag{24}$$

One can include a uniform concentration at the tube surface (isothermal case) or a linear temperature change over the tube length. In the second case, the concentration C_I at the tube wall is a function of z, determined from the temperature dependent saturation curve.

$$T_w(z) = T_{in} + \frac{z}{L}\,(T_{out} - T_{in}) \tag{25}$$

$$C_I(z) = C_{sat}[T_w(z)]\ . \tag{26}$$

3.3 Mass Transfer and Bulk Concentration

The concentration field is used to determine the mass transfer rate and the bulk concentration as functions of the coordinate z in axial direction. Both variables are then used with Eq. (1) to calculate a mass transfer coefficient which is a suitable variable to show the influence of the different system parameters since it depends on the flow conditions only and not on the wall or bulk concentration.

3.3.1 Mass Transfer Rate

The mass transfer rate or, depending on its sign, the corrosion or deposition rate, is described as follows:

$$\dot{m} = D \cdot \frac{\partial C}{\partial r}\bigg|_{r=R}\ . \tag{27}$$

The variables in Eq. (27) and its units used in the code are:

$\dot{m}\ \frac{g}{s \cdot cm^2}$ = mass transfer rate

$D\ (cm^2/s)$ = diffusivity

$C\ (g/cm^3)$ = concentration

$r\ (cm)$ = radius

$R\ (cm)$ = tube radius.

3.3.2 Bulk Concentration

The bulk concentration at the axial position z is defined as:

$$\bar{C}(z) = \frac{\int_0^R C(r,z) \cdot v(r) \cdot dA}{\bar{v} \cdot A} , \qquad (28)$$

with

$$dA = 2r\pi dr$$

$$A = \pi R^2 .$$

3.3.3 Mass Transfer Coefficient

Using the mass transfer rate $\dot{m}$, the bulk concentration $\bar{C}$, and the interface concentration C_I as determined by Eqs. (26) through (28) together with Eq. (1), the mass transfer coefficient is expressed by:

$$K_m(z) = \frac{\dot{m}(z)}{C_I(z) - \bar{C}(z)} . \qquad (29)$$

4. COMPUTER CODE

A first version of a computer code has been developed, based on the model described in Sec. 3, and written in FORTRAN. This code contains a number of simplifications which can be modified in later versions. There also remains a need for an extensive verification process. Calculations for the lithium-lead/ferritic steel system are presented here. It would be beneficial, however, to model corrosion experiments in lithium and sodium since there is a much larger data base available.

In this section the code itself will be described briefly. Section 5 shows a few applications of the code and a description of the input data is given in the Appendix.

4.1 Code Description

The code consists of a controlling main program with ten subroutines which are called sequentially. There are also two function subprograms describing the solubility of the wall material in the liquid-metal and the dynamic viscosity of the liquid metal. These functions currently contain only the properties of lithium-lead alloy. The subroutines are described in the same sequence as they are called by the main program.

4.1.1 Subroutine INPUT

This routine reads in all input data. Each record is printed immediately after it has been read. A description of the input data is in the Appendix.

4.1.2 Subroutine MESH

This routine is called only if the user did not specify the grid in the r- and z-directions. MESH contains default values for the number of grid points and the spacing between the points. Forty-three points are used in the z-direction, 40 to 70 points in the r-direction, depending on the flow pattern and the tube radius.

4.1.3 Subroutine INITIA

INITIA initializes a number of variables using the input data. It calculates the grid spacing and the temperature distribution in the z-direction.

4.1.4 Subroutine VPROFIL

VPROFIL checks the flow pattern (laminar, turbulent, slug flow) and calculates the velocity profile. In the present version the flow profile and the boundary layer thickness are calculated for the highest temperature specified and used for the entire tube.

4.1.5 Subroutine XWALL

XWALL calculates the corrosion product concentration at the surface of the wall, using the solubility function XSATT.

4.1.6 Subroutine DFIELD

DFIELD calculates the molecular and the turbulent diffusivity as it is described in Sec. 3.2.2

4.1.7 Subroutine COEFF

In this routine the elements of the concentration matrix are calculated, using geometrical values prepared by INITIA and the results of the subroutines VPROFIL, XWALL and DFIELD.

4.1.8 Subroutine SOLVE

This routine solves this concentration matrix by use of an over-relaxation method.[10]

4.1.9 Subroutine OUTPUT

In this routine all information contained in the grid spacing, the velocity and concentration profile, and the diffusivities are printed. This output can be suppressed since all information related to the mass transfer itself is printed in the subroutine BALANCE.

4.1.10 Subroutine BALANCE

The main purpose of this routine is to check the accuracy of the calculation.

BALANCE calculates:

(a) the total mass transfer between wall and liquid metal, SCFLUX;

(b) the flux of wall material contained in the inlet flow, FLUXO; and

(c) the flux of wall material contained in the outlet flow, FLUXOUT.

The total accuracy is then determined by

$$\text{RDIFFT} = (\text{FLUXOUT} - \text{FLUXO} - \text{SCFLUX})/\ \text{SCFLUX} \ . \qquad (30)$$

The same check is performed for each axial segment separately.

BALANCE provides a short output containing a summary of all mass transfer related data.

4.1.11 Function XSATT

XSATT specifies the solubility of wall material in the liquid metal as a function of temperature.

$$\text{XSATT} = A \cdot \exp\left(-Q/(R \cdot T)\right) \ , \qquad (31)$$

where

A,Q = material constants

R = gas constant.

The following values are used in the present version for lithium-lead:

A = 9 g/g

Q/R = 13000 K

XSATT is the weight concentration in g/g. This value must be multiplied by the liquid-metal density to obtain the concentration in g/cm^3.

4.1.12 Function DYNVIS

DYNVIS specified the dynamic viscosity of the liquid metal. Since there are no data available for lithium-lead, lead data are used in the present version, approximated by a linear equation.

$$\text{DYNVIS} = 0.057 - 0.5 \times 10^{-4} \times T \ , \qquad (32)$$

where T is the temperature in °K and DYNVIS is the dynamic viscosity in g/cm-s.

4.2 Storage and Computing Time

All arrays in the code are dimensioned dynamically. The storage requirement can therefore be related to the total number of grid points. A rough estimate is

Storage requirement = No. of grid points x 20 + 20000 (bytes) .

All test runs have been performed on a CDC 7600 computer. The CPU time for typical cases with 1000 to 2000 grid points were in the range of 1 to 5 s.

5. APPLICATION OF THE COMPUTER CODE

The main purpose of the code development was to study the influence of some important parameters on the corrosion/deposition rate. This has been done by using the MARS blanket as an example. But prior to this application an attempt has been made to model the conditions in an existing lithium-lead loop for corrosion experiments to see if the corrosion rates predicted by the code are realistic.

5.1 Modeling of the Conditions in a Forced Convection Lithium-Lead Loop

The results of only one forced convection lithium-lead loop have been reported.[4] This experiment has been performed at the Argonne National Laboratory. Corrosion rates where measured on austenitic and ferritic steel specimens. Table 1 shows the measured results for the ferritic specimens.

Table 1

Measured Weight Loss for Ferritic Probe in Lithium-Lead

	Material			
	HT-9		9Cr-1Mo	
	Temperature		Temperature	
Time (h)	427°C	454°C	427°C	454°C
	Weight Loss (g/m^2)			
570	3.81	5.47	3.50	5.94
1450	7.39	13.53	6.74	11.55
2310	11.09	20.06	10.74	17.48
3258	15.45	28.51	15.77	24.97
Average weight loss $\frac{mg}{m^2 \cdot h}$	4.76	8.75	4.86	7.69

The arrangement of the test specimen in the test section is shown schematically in Fig. 2.

The specimens are foils with the dimensions 70 x 10 x 0.3 mm. They are arranged in groups of three. All reported weight changes are the average values of a group. The three specimens expose six surfaces to the flowing liquid metal. Four of the six surfaces are in the narrow gap with a hydraulic diameter of 0.4 cm, the other two have an equivalent hydraulic diameter of 1.5 cm. This complicated geometry is not really suitable for modeling. If it is possible at all to convert this arrangement to a single hydraulic diameter, a value of 1 cm would be a reasonable compromise.

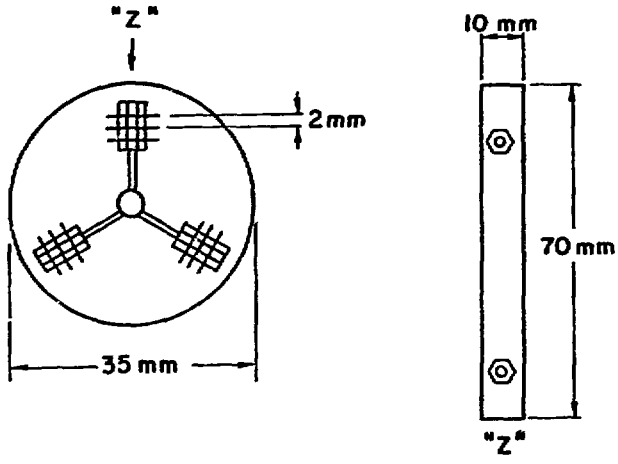

Fig. 2. Arrangement of the test specimen.

The velocity at the probes has not been measured, however a rough estimate of $\bar{v}$ = 3 cm/s is reported in Ref. 11. This estimate leads to a Reynolds number of 1400. It is clear, that the flow conditions were laminar, even if one takes into account all uncertainties in regard to the geometry and the velocity.

A direct extrapolation of corrosion rates measured in laminar flow to the turbulent region is difficult and has a high degree of uncertainty. It should be possible to improve this extrapolation by using a model which takes into account the change in flow pattern.

Additional uncertainty arises from the temperature measurement since there are indications of modest (~5%) temperature variations along the specimen. In all calculations it has been assumed that the temperature is constant over the entire specimen. The following parameters have been used as a base case in the calculations:

Diameter	1 cm
Length	7 cm
Velocity	3 cm
Temperature	727 K (700 K).

Additional scoping calculations have been performed using hydraulic diameters varied in the range between 0.4 cm and 1.5 cm. In some calculations a velocity of 1 cm/s is used since this lower velocity is more typical for the narrow gap between the specimens. The velocity has been varied in a wide range especially to show the influence of a transition from laminar to turbulent flow.

The results of all calculations will be shown as mass transfer coefficients. Therefore, they will not depend on the bulk concentration or the solubility of wall material in the liquid metal. For illustration only a second abscissa is added, showing the corrosion rate. The bulk concentration used for this conversion is the mean value of the saturation concentrations at the hot leg and the cold leg temperature. This takes into account that there was no cold trap in the loop and therefore the iron concentration could build up until an equilibrium between corrosion and deposition was reached. The cold leg temperature was 300°C in all tests.

5.1.1 Influence of the Specimen Length and the Hydraulic Diameter

In Fig. 3 the local mass transfer coefficient is plotted versus the distance from the tube inlet, using the hydraulic diameter as a parameter. The velocity is 3 cm/s in all cases. It can be seen that the mass transfer coefficient decreases fast with increasing distance and that even after 20 cm an asymptotic value is approached. The mass transfer coefficient increases with decreasing diameter due to the larger velocity gradient near the wall surface.

Both effects, the strong influence of the hydraulic diameter and the distance from the inlet on the mass transfer, make the application of the results of corrosion tests performed in the laminar region to general cases rather difficult. Both effects are much smaller in the turbulent region as it can be seen by comparing Figs. 3 and 4.

Considering the precision obtainable in corrosion experiments it is possible to neglect the influence of hydraulic diameter and specimen length if the experiments are performed in turbulent flow. In the case of laminar flow, the effect is too large to be neglected.

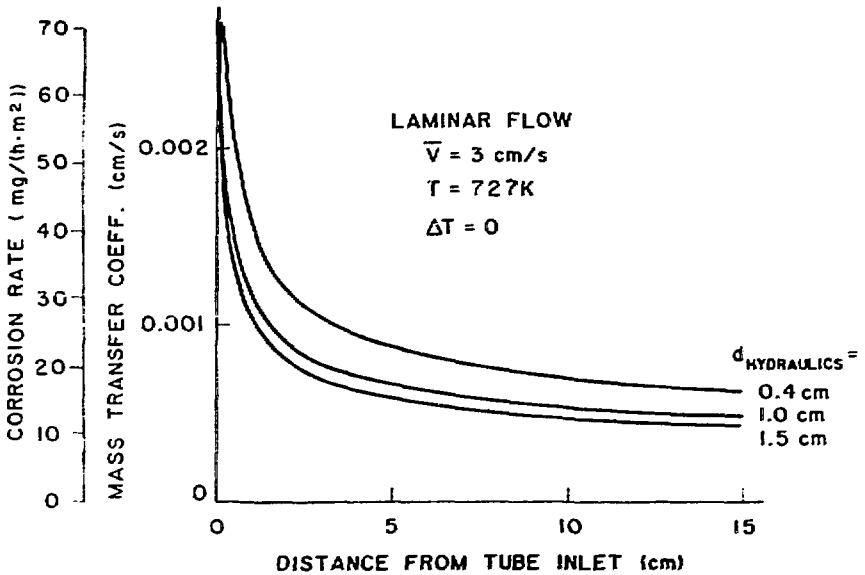

Fig. 3. Mass transfer coefficient as a function of the distance from the flow inlet in the case of laminar flow.

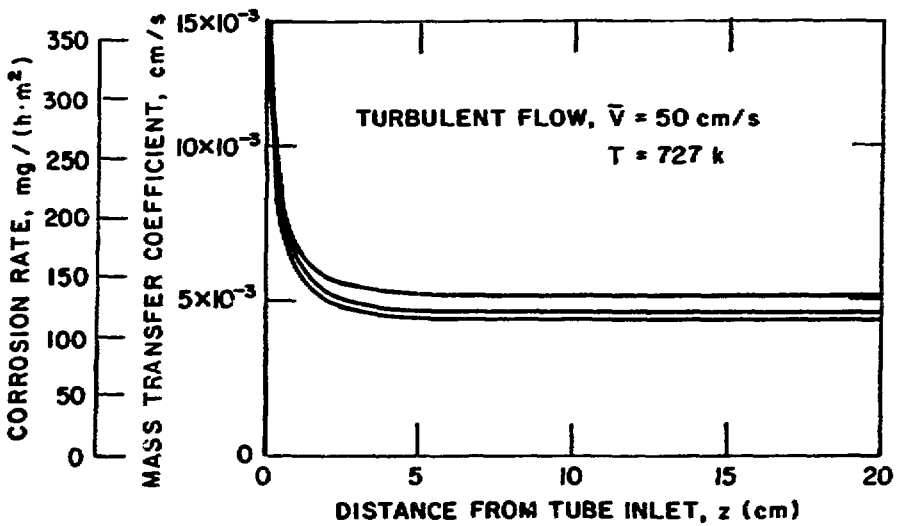

Fig. 4. Mass transfer coefficient as a function of the distance from the flow inlet in the case of turbulent flow.

5.1.2 Influence of the Velocity and the Flow Pattern

This investigation has been performed using a hydraulic diameter of 1 cm and a temperature of 727 K. The critical Reynolds number is reached at a velocity of 5 cm/s but in one set of calculations the program has been forced to stay in the laminar region even if the critical Reynolds number is exceeded. The mass transfer coefficient is calculated at an arbitrarily fixed axial position of z = 7 cm. At this position the mass transfer coefficient has reached its constant value in the turbulent cases, but to reach a constant value in the laminar case a few meters of flow length would be necessary.

The results, which are plotted in Fig. 5, show the mass transfer coefficient as a function of the velocity. An additional line in this diagram shows the velocity dependence as recommended in Ref. 11. This velocity dependence is obtained from sodium experiments since sufficient data does not exist for lithium or lithium lead.

Figure 5 shows clearly that the corrosion rate increases much faster with increasing velocity after the transition from laminar to turbulent flow. Results of this calculation indicate that the use of the velocity dependence function derived from sodium experiments will underpredict the corrosion rate at higher velocities.

Considering the large difference in slope between the laminar and the turbulent curve in Fig. 5, it also does not appear reasonable to extrapolate results of a test in the laminar region to a turbulant case or vice versa.

5.1.3 Comparison of Measured Corrosion Rates with Model Predictions

The corrosion rates for the two ferritic steels, HT-9 and 9Cr-1Mo, as reported in Ref. 4 and listed in Table 1 are plotted in Fig. 6. Usually corrosion rates are represented by the equation:

$$\dot{m} = A \cdot e^{-Q/(R \cdot T)} \quad . \tag{33}$$

In this equation the activation energy represents the temperature dependence. It was not felt appropriate in Ref. 11 to determine Q from the four existing data points since the temperature range investigated in the experiment was rather small. It is suggested instead to use an activation energy of 36 K cal/mole as it has been determined in sodium experiements. A data fit using this activation energy is included in Fig. 6.

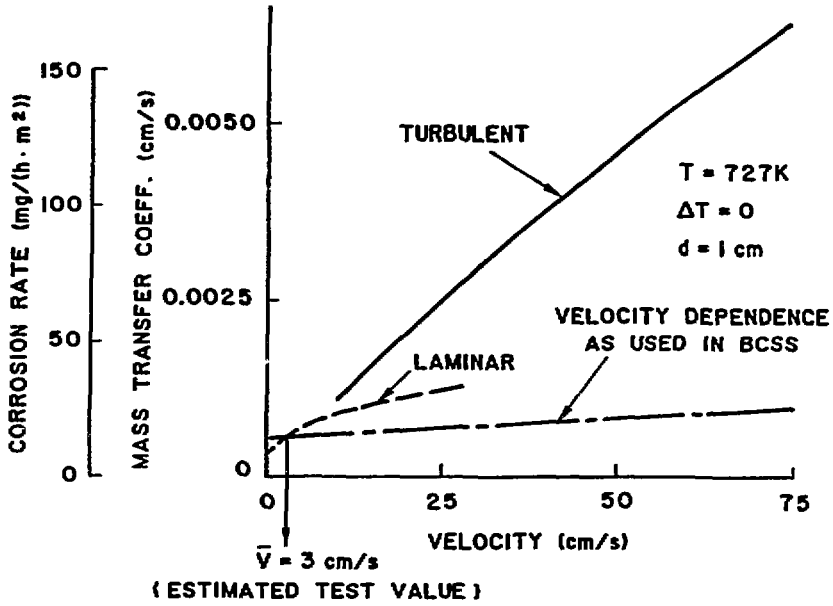

Fig. 5. Influence of velocity and flow pattern (laminar, turbulent) on the corrosion rate.

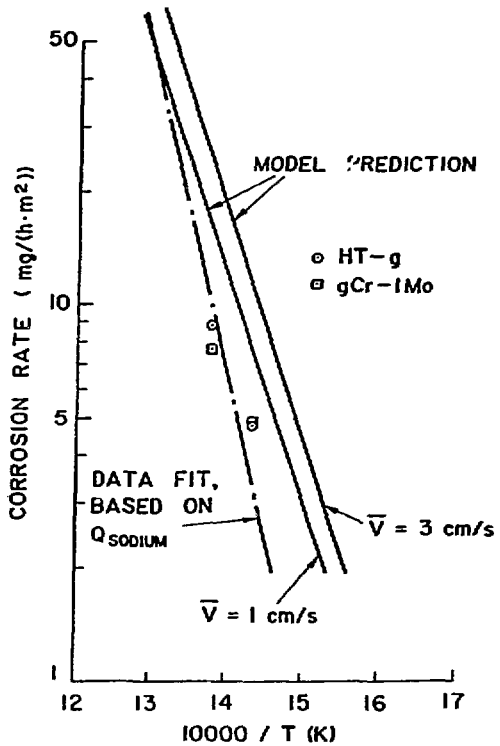

Fig. 6. Comparison between calculated and measured corrosion rates for the case of a forced convection loop experiment.

To obtain the model prediction for the comparison with the experimental results, assumptions have been made in regard to the hydraulic diameter and the velocity. Figure 3 showed that the smaller hydraulic diameter in the narrow gap should lead to a corrosion rate about 50% higher than at the surfaces with the larger hydraulic diameter. However, the measured weight changes of the three specimen showed no significant difference. This indicates that the velocity in the narrow gap was lower than the average value as might be expected from pressure drop considerations. There are also indications that the velocity near the specimen at the higher temperature was somewhat lower than that near the lower temperature specimen. Therefore, calculations have been performed using velocities of 3 cm/s and 1 cm/s. The hydraulic diameter in both cases was assumed to be 1 cm.

An average value of the corrosion rates over the specimen length of 7 cm is calculated, using the assumption that the bulk concentration is the mean value between the saturation concentrations at the hot leg and cold leg temperature.

A comparison of measured and calculated corrosion rates as plotted in Fig. 6 shows that the model predictions are higher by a factor bewteen 1.5 and 3, depending on the velocity assumed. This deviation is suprisingly low, considering all the uncertainties in geometry, velocity and temperature distribution. It should be mentioned here, that the model has <u>not</u> been adjusted by experimental results and that the boundary conditions used in the calculation represent the best judgment of the experimental conditions.

5.2 Modeling of the Corrosion in the MARS Blanket

One of the main objectives of the Mirror Advanced Reactor Study[12] was to design an attractive tandem mirror fusion reactor producing electricity. Lithium-lead has been chosen as breeder and as coolant. All the details of the blanket design can be seen in the MARS Interium Design Report.[12]

The parameters which are important for the liquid metal corrosion in the blanket are listed in Table 2.

Table 2

Blanket Parameter for MARS

Tube inner diameter	9.68 cm
Tube wall thickness	0.23 cm
Tube length (inner row)	180 cm
Average velocity	16 cm/s
Inlet temperature	350°C
Outlet temperature	500°C

Using these parameters as a base case, the following effects have been investigated: (a) the influence of the magnetic field on the corrosion rate in a blanket; (b) the influence of the velocity profile on mass transfer; (c) the variation of corrosion rate along the tube length; (d) the influence of the heat-up rate on the corrosion rate; and (e) the influence of the velocity profile on mass transfer. Similar to the case described in Chap. 5.1 the calculated mass transfer coefficient will be used as a measure for the corrosion rate. Therefore, the results are not influenced by the solubility of the wall material in the liquid metal or by the bulk concentration. This is in agreement with the objective of this study, i.e. to show the influence of the important parameters rather than absolute values of the corrosion rate.

5.2.1 Influence of the Magnetic Field

There have been rather controversial speculations about the influence of the strong magnetic field in a fusion reactor blanket on the liquid-metal corrosion, especially since there are no experimental results available. One possible mechanism is the trapping of ferromagnetic particles. This has been observed many times in electromagnetic pumps used in liquid metal loops.[13,14] Specially designed magnetic traps are used to avoid plugging of these pumps.[13] Magnetic traps might also be used in a fusion reactor to remove corrosion products. This question will be dealt with in Chap. 6.

An indirect influence of the magnetic field is caused by the changes in the flow pattern, namely: (a) the velocity profile becomes very flat, and (b) all turbulence in the fluid is suppressed. The corrosion model is suitable to

investigate the influence of these changes in the flow pattern. This flow pattern will be investigated in the next section together with the laminar and turbulent case.

5.2.2 Influence of the Velocity Profile and the Turbulence

The wall material that goes into solution at the wall/liquid-metal interface, must be transported away. Under certain conditions, this transport which occurs by diffusion perpendicular to the wall surface and by convection parallel to the surface will determine the corrosion rate.

The convective transport depends strongly on the velocity profile. Flat profiles where the average velocity is reached very close to the surface lead to a mass transfer considerably higher than in the case of a parabolic velocity profile typical for laminar flow. The extreme case is a slug flow profile with a uniform velocity and zero boundary layer thickness. Three typical velocity profiles are shown in Fig. 7.

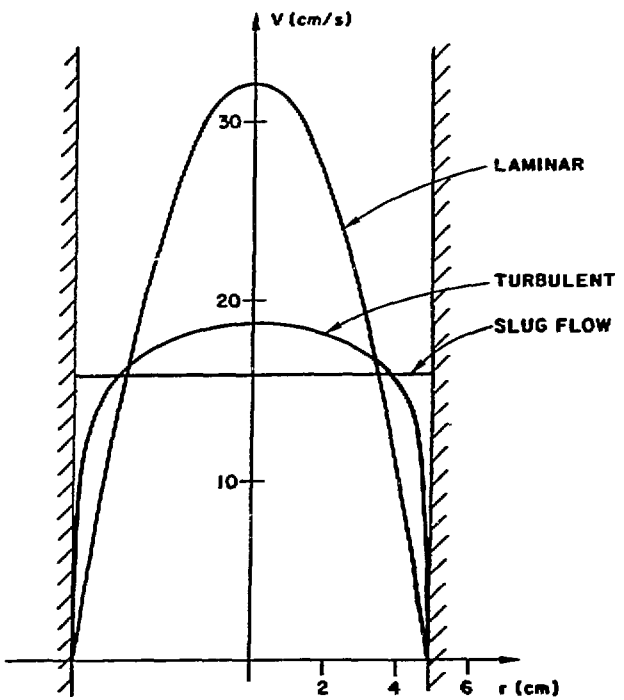

Fig. 7. Typical velocity profiles in tube flow.

The transport by diffusion depends on the total diffusivity, which is the sum of molecular diffusivity and the turbulent or eddy mass diffusivity. In turbulent flow there is always a laminar sublayer with molecular diffusion only. It is obvious that the turbulence can influence the mass transfer only if there is a concentration gradient in the turbulent region. Therefore, it takes a certain flow path length before the turbulence increases the mass transfer compared to a case with an identical velocity profile but without turbulent mass exchange. This can be seen in Fig. 8 which shows the mass transfer coefficient as a function of the distance from the tube inlet. There are four cases included in this diagram: (a) laminar velocity profile; (b) turbulent velocity profile, turbulent mass exchange; (c) turbulent velocity profile, molecular diffusion only; and (d) slug flow profile (uniform velocity), molecular diffusion only (typical for flow in magnetic field).

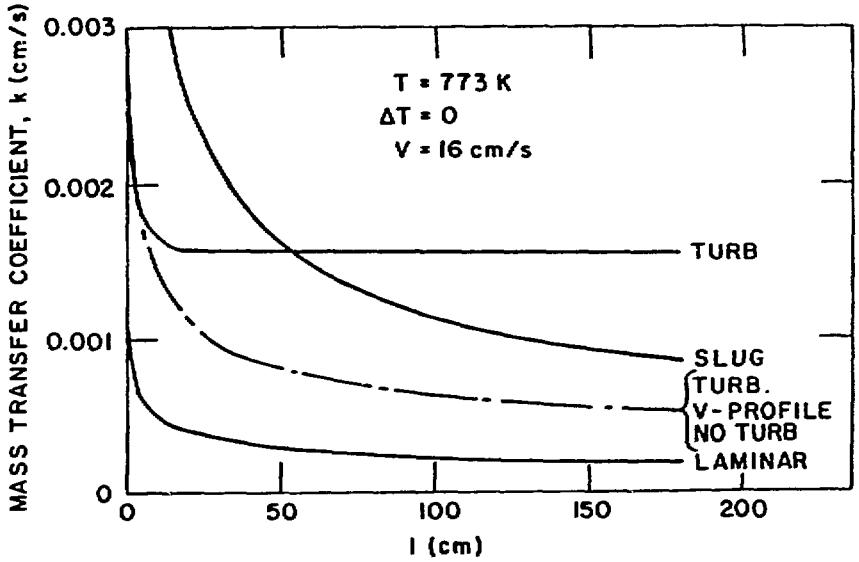

Fig. 8. Influence of the velocity profile on the mass exchange coefficient.

The same average velocity of $\bar{v}$ = 16 cm/s been used in all cases. Using a tube diameter of 9.68 cm and a temperature of 773 K, the Reynolds number is 66000. Boundary layer thickness, velocity distribution and diffusivities are calculated for this Reynolds number using the Eqs. (5) through (13). The boundary layer thickness has been assumed as zero for the slug flow case. Boundary condition is a constant concentration at the liquid-metal/wall interface; that means no temperature gradient in axial direction.

It can be seen in Fig. 8 that the mass transfer increases in the sequence laminar → turbulent → slug flow velocity profile if there is no turbulent mass exchange. The diagram shows that in all three cases the mass transfer coefficient decreases fast with increasing distance from the tube inlet but it does not reach an asymptotic value at a tube length of 180 cm. However, if the turbulent mass exchange is included, the mass transfer coefficient deviates from the case without turbulence after a flow path length of 5 cm and assumes a constant value after 20 cm.

It is interesting to note that the case with the slug flow profile without turbulent mass exchange leads to a mass transfer coefficient considerably higher over the first 50 cm of tube length than the case with turbulent flow. The reason for this surprising result is that in the entrance region the higher velocity close to the wall surface has a larger influence than the turbulent mass exchange. It will be shown in the next section that this remains true over the entire length of the blanket tube if there is a temperature increase in the axial direction.

5.2.3 Influence of a Temperature Gradient in the Axial Direction

It has been shown in the preceding section for the case of isothermal flow that the mass transfer coefficient decreases over the entire tube length with the exception of turbulent flow, or in other words, that the entrance region is longer than the whole assumed blanket tube. Therefore, the effect of the entrance region must be taken into account for the relative large ratio tube diameter/tube length typical for a fusion reactor blanket. This is even more pronounced by a temperature gradient in axial direction. Therefore, the application of empirical mass transfer equations, verified for fully developed concentration profiles only, would be misleading.

The model predictions for the MARS blanket are shown in Fig. 9. The results of all the different cases as listed in Fig. 9 are represented as normalized mass transfer coefficients at the tube outlet. The slug flow case with a 10-μm boundary layer thickness is set at 100% because this is the most likely case for the blanket. A 10-μm boundary layer thickness has been chosen in order to account for assumed surface roughness.

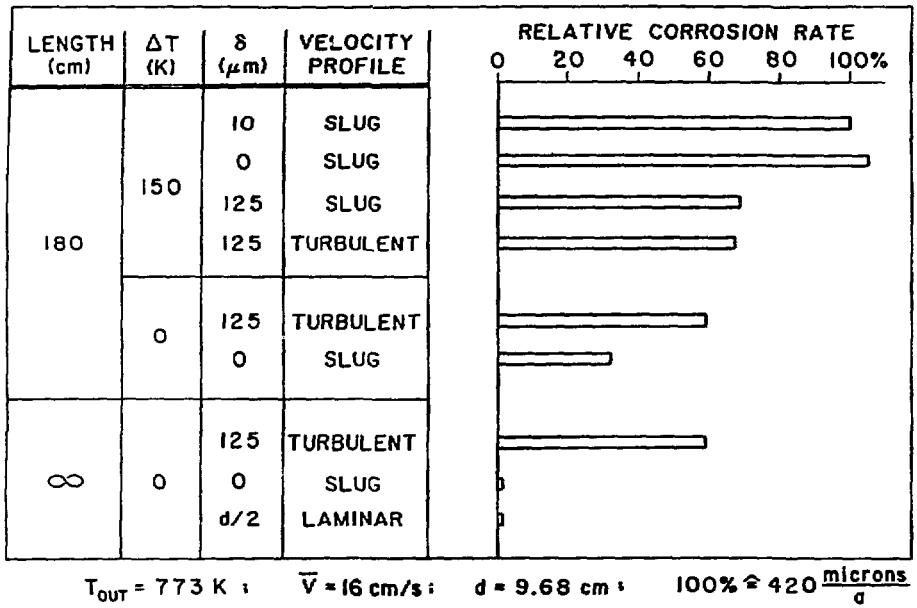

Fig. 9. Influence of tube length, heat-up rate, velocity profile, and boundary layer thickness on the corrosion rate.

The parameters listed in Table 2 are kept constant in all cases. Varied are the velocity profile and, in the case of slug flow, the boundary layer thickness. Included for comparison are isothermal cases with 180 cm tube length as shown in Fig. 8, and the theoretical predictions for an isothermal, infinite long tube with both laminar and slug flow velocity profiles.

It can be seen that a change from 10 μm to zero boundary layer thickness has only a small influence, but that a layer of 125 μm reduces the mass transfer by 32%. A larger boundary layer reduces the velocity near the wall surfaces, and therefore, the mass transfer. Figure 10 shows the influence of the boundary layer thickness on the mass transfer coefficient for the slug flow case.

A comparison of the isothermal cases with the ones having a temperature increase of 150 K shows the influence of the temperature increase on the entrance region. It can be seen that the mass transfer in the turbulent cases does not vary much but that the influence of the entrance region is large in the case of slug flow.

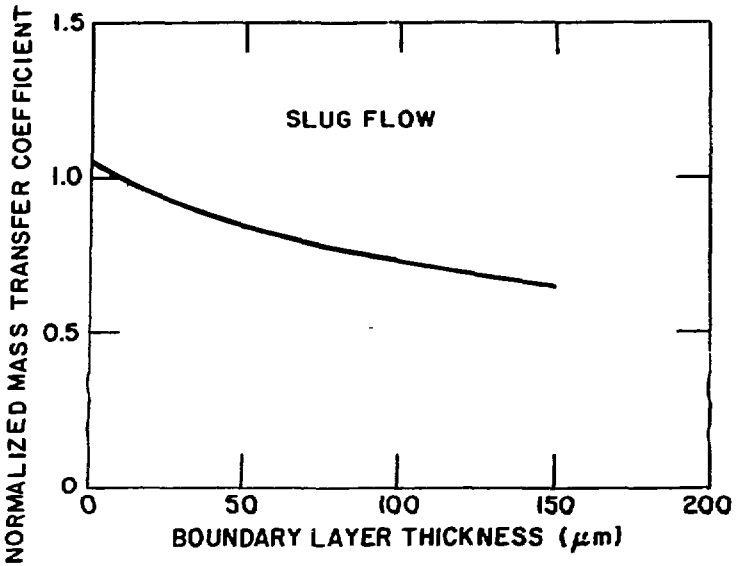

Fig. 10. Mass transfer coefficient as a function of the boundary layer thickness.

5.2.4 Influence of the Liquid-Metal Velocity

In Fig. 11 the normalized mass transfer coefficient at the outlet is plotted as a function of the average liquid-metal velocity. Outlet temperature and temperature rise have been kept constant. This is not the case for a given blanket design because the temperature rise is determined by the velocity if volumetric heat generation and tube length are kept constant.

The velocity dependence of the mass transfer for constant heat generation and outlet temperature is shown in Fig. 12. This diagram shows the result of calculations where the product of velocity and temperature rise has been kept constant. It can be seen that the mass transfer coefficient under these conditions shows only a slight velocity dependence.

5.2.5 Influence of the Outlet Temperature

The temperature dependence of the mass transfer has been separated from the influences of magnetic field, velocity profile, turbulence, temperature gradient and velocity. Therefore, all these influences could be shown by using a normalized mass transfer coefficient as a scale. This scale, however,

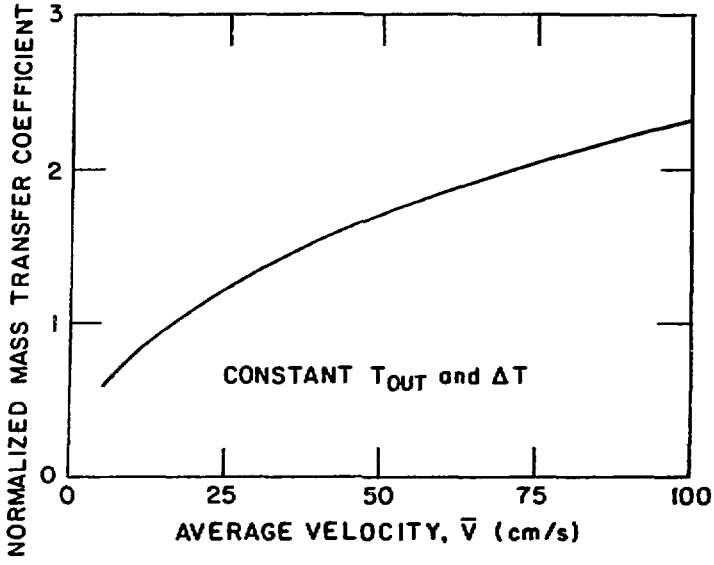

Fig. 11. Mass transfer coefficient as a function of the average velocity.

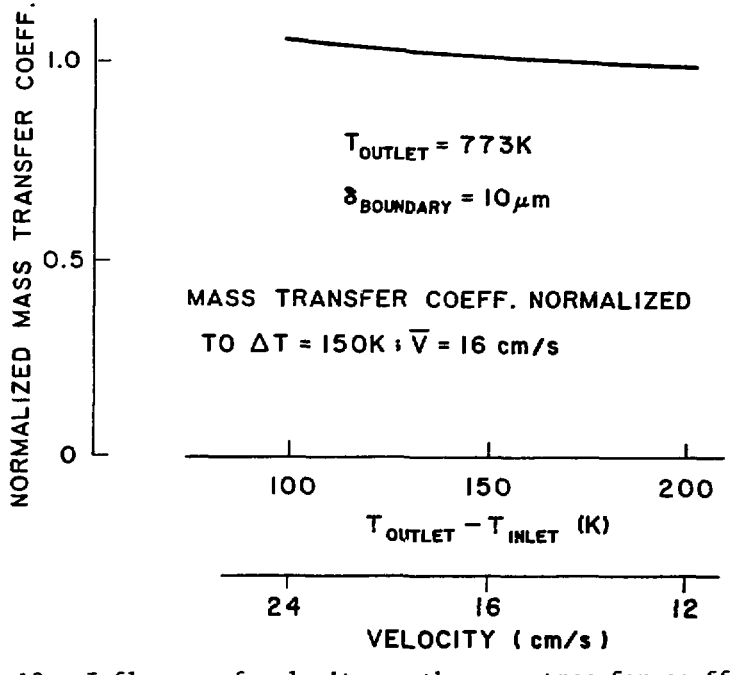

Fig. 12. Influence of velocity on the mass transfer coefficient for constant heat generation and outlet temperature (inlet temperature variable).

would not be a meaningful one in showing the influence of the outlet temperature because it would reflect only the changes in diffusivity and viscosity. The much stronger influence results from the change in saturation concentration which depends much stronger on the temperature than the other material properties. Therefore, the calculated corrosion rates for different outlet temperatures have been normalized by the rate at 500°C. The base case is identical to the one used in the previous sections (slug flow, 10-μm boundary layer, 150 K temperature rise, 3-cm/s velocity).

Figure 13 shows the normalized corrosion rate as a function of the outlet temperature. The absolute value of the corrosion rate as predicted by the model will be shown in the next section.

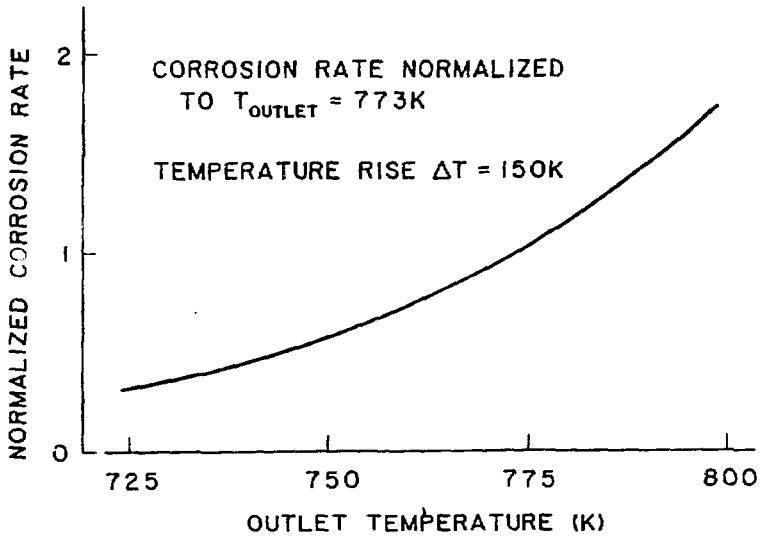

Fig. 13. Influence of the outlet temperature on the corrosion rate.

5.2.6 Absolute Values of Mass Transfer Coefficient and Corrosion Rate

The objective of this study is to investigate the influence of the important parameters on the corrosion rate. This has been accomplished by using the mass transfer coefficient as a relative scale. There remains, however, a desire to obtain absolute values of the corrosion rate. The model calculates corrosion rates but as long as it is not verified on suitable experiments, absolute values are far more speculative than the relative influences.

There is another problem involved in reporting the calculated corrosion rates. Mass transfer coefficients can be calculated for a single pipe but the entire liquid-metal loop must be investigated in order to obtain meaningful corrosion rates. The reason for this is that the corrosion rate does not depend only on the local mass transfer coefficient and the interface concentration but also on the bulk concentration in the liquid-metal flow. This bulk concentration depends on the ratio of cold and hot surface area on the flow conditions in the entire loop and on many other design variables. For all these reasons the corrosion rate as calculated by the model should be looked at with the necessary caution.

The base case used in all normalizations is characterized by the variables as listed in Table 2 and by:

- slug flow velocity profile,
- boundary layer thickness 10 μm.

It results in:

- mass transfer coefficient at the outlet

$$K_m = 2.62 \times 10^{-3} \text{ cm/s} ,$$

- corrosion rate at the outlet

$$\dot{m} = 1.03 \times 10^{-8} \text{ g/s} \cdot \text{cm}^2 = 370 \text{ mg/m}^2 \cdot \text{h} .$$

In determining this corrosion rate the assumption has been made that the liquid metal is saturated with wall material at 673 K, a temperature 50 K higher than the inlet temperature.

5.3 Modeling of Corrosion Product Deposition

The modeling of material deposition is identical to the modeling of dissolution. In a real liquid metal loop; however, there is an important difference in the transient behavior of the two processes. Corrosion increases the flow area, leading to a lower velocity and as a consequence to a lower corrosion rate. Usually this negative feedback of corrosion can be neglected. In the case of deposition, however, this feedback is positive and can become so large that it results in a complete plugging of a loop. A typical place where this occurs is the smallest cross section in a valve. The problem of enhanced

deposition rate is pronounced by the fact that an acceleration of the flow is accompanied by a flattening of the velocity profile and a thinning of the boundary layer. Deposition mass transfer should be investigated; therefore, especially in the entrance region of flow reductions, such as at the beginning of the smallest flow cross section. It is a realistic assumption that there is a uniform velocity over the cross section with a very thin boundary layer. The use of a slug flow profile with zero boundary layer thickness has the additional advantage that it leads to the highest possible deposition rate. There is no influence of either tube diameter or turbulence on the mass transfer in this region, provided the length of the section is not more than a few times the diameter.

The computer code described in Sec. 4 has been used to calculate deposition rates in the following case:

- wall temperature (isothermal) 623 K
- uniform concentration at the inlet
- slug flow velocity profile.

The results of these calculations are shown in Fig. 14. Plotted is the mass transfer coefficient as a function of the distance from the inlet with the velocity as parameter. Included for comparison is the case of a turbulent velocity profile.

A second abscissa in this diagram shows the deposition rate in μm/y, based on the assumption that the liquid metal is saturated at 673 K, a temperature 50 K higher than the wall temperature. It can be seen that the deposition rate decreases over a few cm from a high value at the inlet to values below 100 μm/y. This decrease is much faster if a turbulent velocity profile is assumed.

The deposition rate is also decreased if a boundary layer is assumed in the slug flow case. This can be seen in Fig. 15, which shows the conditions at a distance of 2 cm from the inlet as a function of the boundary layer thickness. The velocity in this case is 50 cm/s.

Considering the large flow areas in the primary loop of a liquid metal blanket, the deposition rates over most of the length shown in Fig. 14 and 15 are not prohibitive large. However, the result indicates highly localized

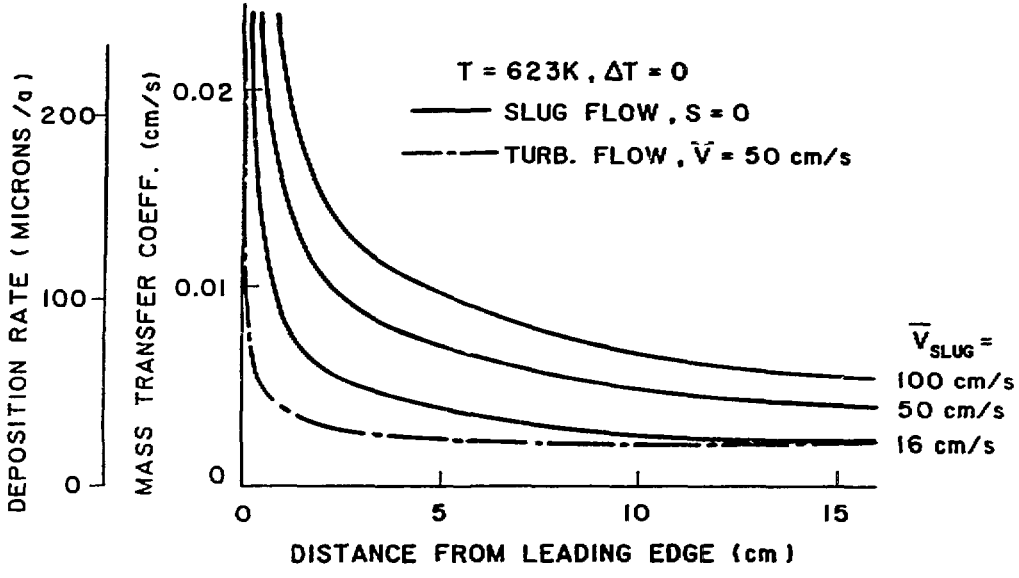

Fig. 14. Deposition rate as a function of the distance from the leading edge.

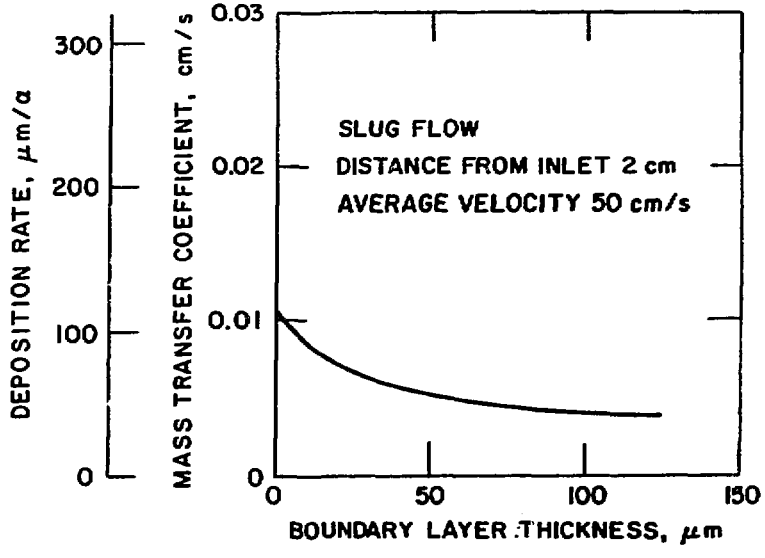

Fig. 15. Deposition rate as a function of the boundary layer thickness.

deposition at the inlet. It may be possible to taper necessary cross-section reductions in a way to avoid excessive changes in flow cross sections over the lifetime of components. However, valves, sharp bends, and other restrictions could pose serious problems.

6. CORROSION PRODUCT CONCENTRATION IN THE LIQUID-METAL FLOW

If a loop is filled the first time with liquid metal, the concentration of wall material in the liquid metal is negligible. The dissolution of wall material in the high-temperature region leads then to a gradual concentration buildup because a certain amount of wall material is added each time the liquid metal passes through the high-temperature region. After a certain time the saturation concentration is reached at the location of the lowest liquid-metal temperature. Starting at this moment, wall material will be deposited at colder parts of the loop. A steady-state condition is reached when the amount of material deposited equals the amount dissolved. This qualitative description is valid for all components of the wall material. But the time to reach saturation and the amount of material transferred are completely different for each component since the solubility varies by orders of magnitude. This quantitative difference will be shown in Sec. 6.1 for the components iron and nickel. In a real case the deposition process is more complicated by the formation of compounds of single components. It has been observed, for example, that deposition of a compound of nickel and manganese occurs long before the solubility limit of nickel is reached.[13] The analysis of the behavior of such compounds, however, is beyond the scope of this study. This is one more reason why the direct application of this study is limited to the case of ferritic wall materials where the corrosion/deposition behavior is governed by the solubility of iron.

Numerically, dissolution and deposition rates are calculated as the product of concentration difference times mass transfer coefficient. The determination of the mass transfer coefficient as a function of the flow conditions has been shown in Sec. 5. The other factor is the difference between the concentration at the liquid-metal/wall interface and the bulk concentration in the flow. Section 6.2 shows how the bulk concentration and, therefore, the balance between wall thinning and deposition can be influenced by a suitable design of a corrosion product cleanup system.

6.1 Difference in the Deposition Behavior Between Nickel and Iron

There are no data available for the solubility of iron and nickel in 17Li83Pb. As an estimate, the solubilities in lead of these elements will be used. They are plotted in Fig. 16. The slope of the iron-line in this Arrhenius plot is steeper than the one for nickel but the deposition rates predicted by the model depends more on the absolute concentration than on the slope of the solubility.

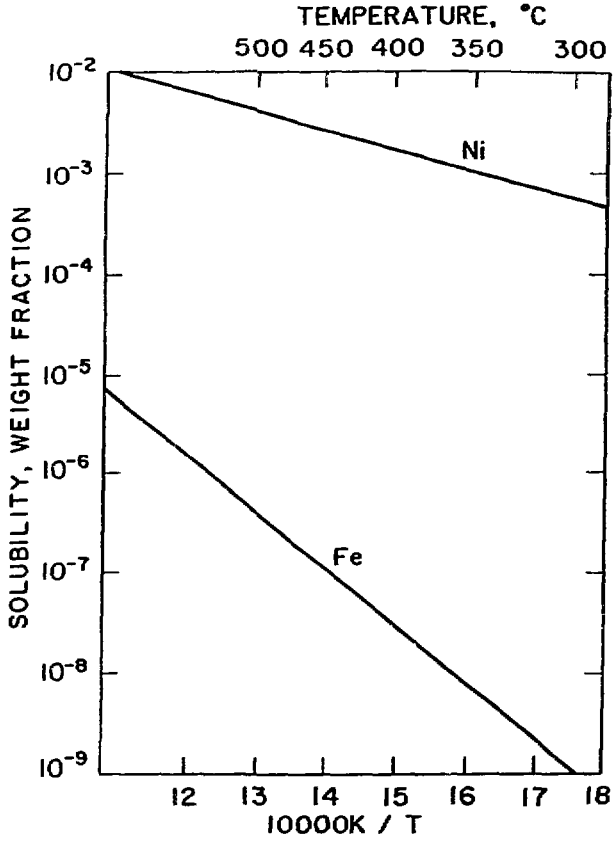

Fig. 16. Solubility of iron and nickel in lead.

This effect is demonstrated by the following example, which uses the temperature range of the MARS blanket. Let us assume that the liquid metal having a density of 9.4 g/cm^3 is saturated at 673 K in one case with nickel, in

the other case with iron. The question then is how much iron or nickel, respectively, will be deposited if the temperature is lowered to 623 K and no supersaturation is allowed. Table 3 shows the solubilities at these temperatures.

Table 3

Solubilities of Iron and Nickel in Lead

	Iron	Nickel
Weight fraction X_{673} at 673 K	36.7×10^{-9}	1.78×10^{-3}
Weight fraction X_{623} at 623 K	7.8×10^{-9}	1.05×10^{-3}
$\Delta X = X_{673} - X_{623}$	28.9×10^{-9}	0.73×10^{-3}
$\Delta C = \Delta X \cdot \rho(g/cm^3)$	0.27×10^{-6}	6.86×10^{-3}

If the flow conditions and, therefore, the mass transfer coefficient are the same in the nickel and the iron case, iron would be deposited at a rate lower by a factor of 25000 than nickel. This factor increases to 75000 if a saturation temperature of 623 K and a wall temperature of 573 K is assumed.

It is important to keep this relationship between the two elements in mind if the experience with deposits and cold trap systems in existing liquid-metal loops is applied to a fusion reactor blanket. In most cases where deposits caused a problem and were analyzed, they contained a large fraction of nickel.[13]

A rough estimate, however, indicates that the nickel concentration in the primary loop of the ferritic steel MARS blanket would not reach the saturation concentration at the inlet temperature, even if all the nickel contained in the entire blanket and in all steam generator tubes would go into solution. Provided this picture will not change completely if the formation of nickel-manganese compounds is considered too, deposition of nickel would be of no concern in a blanket with ferritic steel as structure material.

The result is completely different if austenitic steels are used, and may be different in a small loop constructed of ferritic steel because of the larger surface to liquid-metal volume ratio. For this reason the iron concentration only will be investigated in the following section.

6.2 Buildup and Control of the Iron Concentration in the Liquid-Metal Loop

It has been estimated that the total corrosion rate in the MARS blanket is 0.020 g/s.[12] With a liquid-metal inventory of roughly 10^7 kg, it takes about one hour to reach the saturation concentration at the inlet temperature. This indicates that an equilibrium between the dissoluted and the deposited iron mass is reached in a short time. An important question, however, is at which concentration this equilibrium is reached and where the material is deposited.

Uncontrolled deposits could be avoided if an efficient trap is used that could control the corrosion product content to a level below the saturation concentration at the inlet temperature. An attempt has been made to design such a trap for the MARS blanket. The idea behind this design is to cool the liquid metal in a separate heat exchanger to a level below the inlet temperature, resulting in precipitation of the corrosion products. Due to the high Schmidt number of liquid metals it is theoretically possible to get such precipitation as particles inside the liquid-metal flow rather than as deposits at the wall surface. The idea then is to filter the particles out.

This system would conceivably work for nickel particles. The growth rate of iron particles, however, is so low that the particles are too small to be filtered out. This can be shown on a simple example as follows. It is assumed that there are already iron spheres with a radius r_0 in the liquid metal and that there is no relative velocity between sphere and surroundings. This assumption is justified because the particles are small and the difference in density is not large. In such a case the Sherwood number which determines the mass transfer has a constant value of 2. A growth rate for the sphere can be formulated, using the Sherwood number, the molecular diffusivity and the concentration difference between the supersaturated liquid metal and the sphere/liquid-metal interface. Intergration of this growth rate results in an equation determining the time necessary to increase the sphere radius from r_0 to r_1:

$$t = \frac{r_1^2 - r_0^2}{2 \cdot \Delta X \cdot D} \cdot \tag{34}$$

The result of this equation is plotted in Fig. 17 with the assumption, that $r_0 \ll r_1$ and that ΔX is the difference between the saturation concentrations at 350°C and 310°C as it has been suggested in Ref. 12.

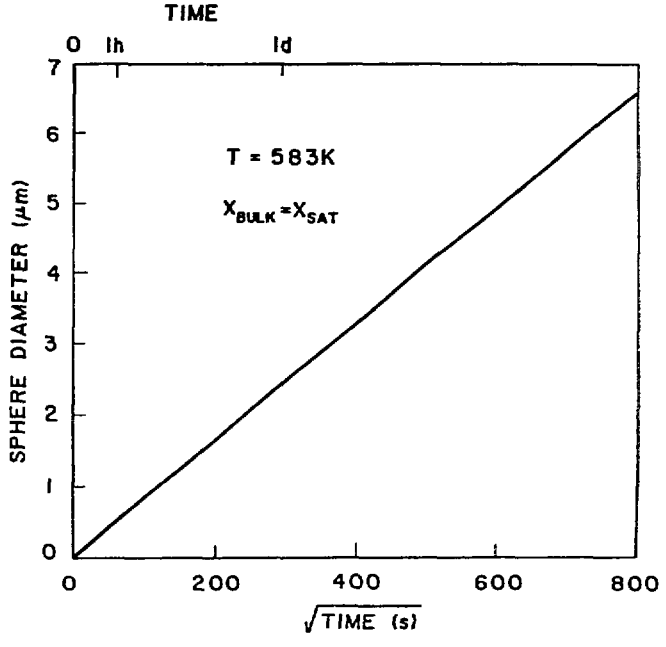

Fig. 17. Growth rate of iron spheres in supersaturated lead.

It can be seen that it takes four days to obtain spheres with 5-μm diameter. Obviously this time is not available. A comparison to an identical case for spheres of nickel is interesting, since for the same diameter the time necessary is only 5 s. The relation of four days for an iron sphere to 5 s for a nickel sphere of equal diameter explains clearly why it is possible to get nickel particles precipitated and filtered out but that iron will be deposited only on surfaces.

A very rough estimate is that 5000-m^2 surface area would be necessary to subsidize for the cleanup system as described in Ref. 12. The volume/surface area ratio for a wire is d/4. This means that a volume of 0.625 m^3 or roughly 5 tons of wire material would be necessary to provide a surface area of 5000 m^2 if a diameter of 0.5 mm is chosen. Assuming that this amount of steel wool fits into a volume of 10 m^3, the total liquid metal would be increased by

roughly 1% if such a trap is added. Additional volume would be required for piping and the heat exchanger.

These estimates are based on the assumption that supersaturation at the inlet temperature must be avoided and, therefore, the liquid metal is cooled down from 350°C to 310°C in a separate heat exchanger. If the bulk concentration is higher, a smaller cleanup system would ideally lower the corrosion rate; however, plugging or trap saturation would occur sooner. This is explained by the following example:

Assumptions:

(a) The limiting corrosion occurs at the blanket outlet under the following conditions:

- temperature 773 K (inlet temperature 623 K)
- tube diameter 9.68 cm
- slug flow
- boundary layer thickness 10 μm
- velocity 16 cm/s

A mass transfer coefficient of 2.62×10^{-3} cm/s has been calculated for this condition:

(b) The most severe deposit occurs in a valve 2 cm downstream from the leading edge under the following conditions:

- temperature 623 K (isothermal)
- slug flow
- no boundary layer
- velocity 50 cm/s

The resulting mass transfer coefficient is 7×10^{-3} cm/s:

(c) The bulk concentration is controlled by the amount of steel wool in the cold leg at 623 K. The surface area necessary to maintain $X_{bulk} = X_{sat}$ (673 K) is assigned a value of 1. A very rough estimate which can give the order of magnitude only is that the absolute value of this area is 1000 m^2 or, using a wire diameter of 0.5 mm, a mass of 1000 kg. This estimate is based on a liquid-metal velocity through

Corrosion and deposition rates at the selected locations are plotted in Fig. 18 as a function of the temperature T_{sat} at which the liquid metal is saturated. Also shown is the predicted surface area in the corrosion product trap necessary to maintain this saturation temperature. These results indicate that it may be possible to control the desired bulk concentration by varying the surface area/volume of the trap. Bulk concentration and flow conditions then determine the corrosion and deposition rates. The allowable limits for both rates are not independent but depend on the particular design. Removal of the corrosion product, i.e., reducing the saturation concentration will tend to increase the corrosion rate. As the maximum temperature is increased, corrosion/deposition rates may increase to the point where trapping would become impractical because of rapid trap saturation.

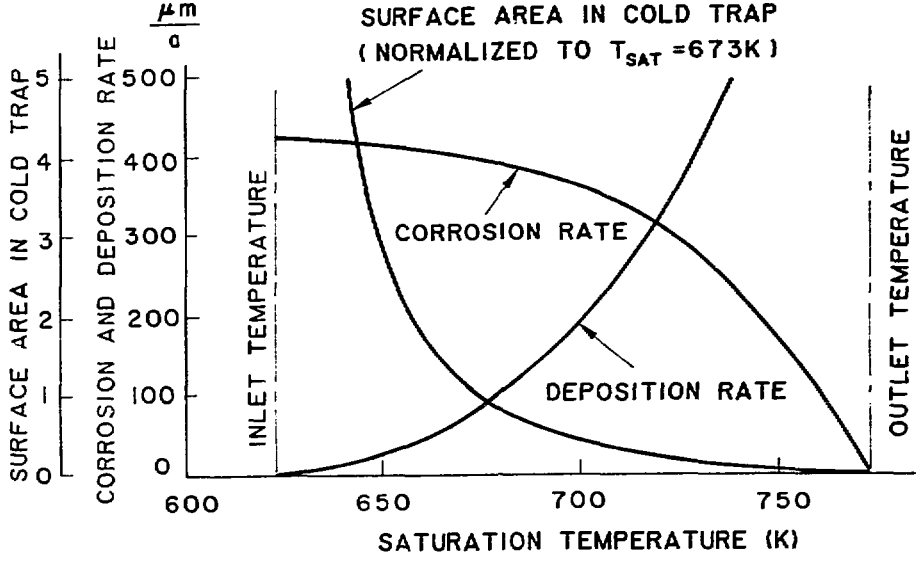

Fig. 18. Corrosion rate, deposition rate, and surface area needed in the cold trap of the MARS blanket loop.

Stress considerations provide a limit for the allowable corrosion rate. Generally the allowance for wall thinning is established as ~10% of the wall thickness. It is more difficult to set a general limit for the deposition. There is a large difference in this limit if it is determined by radioactive mass transport considerations or by the allowable reduction of flow cross-section areas. Preferential deposition in localized regions are predicted.

The deposition rate shown in Fig. 18 is calculated for the smallest cross section of a valve where deposits can lead to plugging. Predicted deposition in the blanket pipe of MARS would be lower at least by a factor of 5.

7. CONCLUSIONS

The application of the corrosion/deposition model developed in this study to a corrosion experiment and to a typical lithium-lead blanket design points out the need for well-defined corrosion experiments. Those experiments should be designed to verify and benchmark models that can then be used to extrapolate the experimental results to specific fusion reactor blanket conditions. It is recognized that there are a number of practical constrains in designing and operating a liquid-metal corrosion experiment. Nevertheless a "wish list" from a modeling point of view may be helpful in defining a reasonable compromise between the practical difficulties and the desire for clearly defined conditions. The most important points are:

(a) Loop design such that corrosion and deposition test specimens can be inserted/removed at the same intervals.

(b) Use of the same type of structural material for the entire loop.

(c) Flow conditions clearly defined over the whole loop but especially at the test specimen locations.

(d) Either length of specimen large enough to neglected entrance region or axial distribution of corrosion/deposition rate measured.

(e) Liquid metal and wall temperature along the test specimen either constant or with a well defined gradient.

(f) Either no corrosion clean up system or a system sufficiently sophisticated that the bulk concentration in the liquid metal after passing the system is known.

An attempt was made to model the conditions in an existing test loop for lithium-lead corrosion of ferritic steel. Although the results have a high degree of uncertainty, the comparison of measured and calculated corrosion rates, indicates that the model predictions are not unreasonable. This gives some confidence in the main results of the study, namely the relative influence of the most important parameters.

The calculations show clearly that the enhanced mass transfer in the region of developing concentration profile has to be taken into account, especially if there is:

- a temperature gradient in flow direction
- turbulence suppressed by a magnetic field
- a small ratio length to diameter (typical for critical areas of mass deposit).

It has been shown for the conditions of the MARS blanket, that the very thin boundary layer caused by the magnetic field outweighs the influence of the suppressed turbulence on the corrosion rate.

Modeling of the deposition behavior of iron and nickel indicates that the deposition rate depends more on the absolute solubility level than on the relative temperature dependence of the solubility. This means that the deposition rate of nickel would be much higher than that of iron if the liquid metal is saturated with the respective element.

An estimate for the case of the MARS blanket shows, however, that the small amount of nickel contained in the ferritic steel structural material (HT-9, 0.5% nickel) is not sufficient to saturate the liquid metal even at the inlet temperature. This would mean that there is no possibility for nickel deposits. However, deposits of a nickel-manganese compound, which have been observed in corrosion experiments, can be explained by a solubility much lower than that of nickel. If this is the case, the deposition rate should be comparable to that of iron as calculated in this study and much lower than the nickel deposition in loops made of austenitic steel.

APPENDIX

Description of Input Data

1. Record — Format (2I10)

NRGROS	(-)	Number of radii to be read in. If the radial mesh has to be set by the code (default option), NRGROS = 1 has to be set.
NZGROS	(-)	Number of axial levels to be read in. If the axial mesh has to be set by the code (default option), NZGROS = 1 has to be set.

2. Record — Format (4(F10.3, I10))

RGROS (K)	(cm)	Cross lattice radius, starting with the outer radius.
KFINE (K)	(-)	Number of fine mesh radii between the RGROS (K) and RGROS (K + 1) (equally spaced).

K = 1, NRGROS

3. Record — Format (4(F10.3, I10))

ZGROS (L)	(cm)	Gross lattice z-coordidate, starting with ZGROS = 0 (inlet). If NZGROS = 1 (default option), ZGROS(1) = tube length has to be set.
LFINE (L)	(-)	Number of fine-mesh z-coordinates between ZGROS (L) and ZGROS (L + 1) (equally spaced).

L = 1, NZGROS

4. Record — Format (8F10.4)

TIN	(K)	Temperture at the tube inlet.
TOUT	(K)	Temperature at the tube outlet.
XIN	(wppm)	Bulk concentration of wall material in the liquid metal at the inlet.

Default options: (a) XIN > 100 XIN = XSATT (XIN)

(b) XIN < 0 XIN = XSATT (TIN)

XSATT (TIN) is the saturation concentration at the temperature TIN.

VMEAN	(cm/s)	Average velocity.

BLAYER	(cm)	Boundary layer thickness. Used only in the case of DTURB < 0 (magnetic field). In the case of turbulent flow without magnetic field, BLAYER is calculated by the code.
RECRIT	(-)	Critical Reynolds number for the transition laminar - turbulence.
DTURB(-)		Control variable for velocity profile and turbulent mass exchange:
		DTURB < 0: Linear increase of velocity between r_0 = RGROS (1) and r_i = RGROS (1) - BLAYER, uniform velocity in the core $r < r_i$, no turbulent mass exchange.
		DTURB $\geq$ 0: Velocity profile, boundary layer thickness and turbulent exchange are calculated, depending on the Reynolds number.
RHOM	(g/cm^3)	Liquid metal density.

5. Record — Format (2F10.4, 3I10)

OMEGA	(-)	Overrelaxation factor 1.0 $\leq$ OMEGA < 2.0.
EPS	(-)	Convergence criteria; recommended EPS = 1.E-7.
KIT	(-)	KIT = Number of iterations; recommended KIT = 500. If KIT < 0, information concerning the convergence is printed for the last iteration step only.
IPRINT	(-)	IPRINT < 1: Results are printed for the outer radius only.
		IPRINT = 1: Results for all radii are printed.
		IPRINT > 1: Results for each IPRINT'TH radius are printed.
UPRINT	(-)	UPRINT > 1: Results for all axial levels are printed.

REFERENCES

1. O. K. Chopra and P. F. Tortorelle, J. Nucl. Mater. 122, 1201 (1984).

2. O. K. Chopra and D. L. Smith, "ADIP Semiannual Progress Report," U.S. Department of Energy Report DOE/ER-0045/11, p. 195 (March 31, 1983).

3. G. A. Whitlow et al., J. Nucl. Mater. 85 & 86, 283 (1979).

4. O. K. Chopra and D. L. Smith, "Corrosion of Ferrous Alloyus in Eutectic Lead-Lithium Environment," Proc. 3rd. Top. Mtg. Fusion Reactor Materials, Albuquerque, NM, September 19-22, 1983.

5. P. E. Tortorelli and O. K. Chopra, "Corrosion and Combatiblity Considerations of Liquid Metals for Fusion Reactor Applications," J. Nucl. Mater. 103 & 104, 621 (1981).

6. M. K. Schad, "Corrosion of Austenitic Steel in Sodium Loops," Nucl. Technol. 50, 67 (1980).

7. A. H. P. Skelland, Diffusional Mass Transfer, Wiley & Son, New York (1974).

8. W. Rohsenow and H. Choi, Mass and Momentum Transfer, Prentice Hall Inc., Englewood Cliffs (1961).

9. W. Jost, Diffusion, Academic Press, New York (1952).

10. D. R. Croft, D. G. Lilley, Heat Transfer Calculations Using Finite Difference Equations, Applied Science Publishers Ltd., London (1977).

11. "Blanket Comparison and Selection Study, Interim Report," Argonne National Laboratory, ANL/FPP/TM-177 (1983).

12. "Mirror Advanced Reactor Study, Interim Design Report," University of California-Los Angeles, UCRL-53333 (1983).

13. O. K. Chopra and D. L. Smith, Argonne National Laboratory, unpublished results (1984).

14. V. Maroni et al., "Analysis of the October 5, 1979 Lithium Spill and Fire in the Lithium Processing Test Loop," ANL-81-25 (1981).

DISTRIBUTION FOR ANL/FPP/TM-192

Internal:

C. Baker
M. Billone
J. Brooks
Y. Cha
O. Chopra
R. Clemmer
D. Ehst
K. Evans
D. Gruen
P. Finn
F. Fradin
A. Hassanein
C. Johnson
J. Jung
T. Kassner
R. L. Kustom
Y. Liu
R. Mattas
B. Misra
K. Natesan
W. Praeg
J. Roberts
D. Smith (5)
D. Sze
L. Turner
FPP Files (10)
ANL Contract File
ANL Libraries
ANL Patent Dept.
TIS Files (6)

External:

DOE-TIC, for distribution per UC-20 (110)
Manager, Chicago Operations Office, DOE
University of Chicago Special Committee for the Fusion Program:
S. Baron, Brookhaven National Lab.
H. K. Forsen, Bechtel National, Inc., San Francisco
J. A. Maniscalco, TRW, Inc., Redondo Beach
G. H. Miley, U. Illinois, Urbana
P. J. Reardon, Brookhaven National Lab.
P. H. Rutherford, Princeton U.
D. Steiner, Rensselaer Polytechnic Inst.
K. R. Symon, Synchrotron Radiation Center, Stoughton, Wis.
K. I. Thomassen, Lawrence Livermore National Lab.
W. Bjorndahl, TRW, Inc., Redondo Beach
J. DeVan, Oak Ridge National Lab.
N. Hoffman, Energy Technology Center, Canoga Park
S. Malang, Kernforschungszentrum Karlsruhe, Federal Republic of Germany (5)
D. Oleson, Colorado School of Mines
P. Tortorelli, Oak Ridge National Lab.